NANO LETTERS

2007
Vol. 7, No. 6
1505−1511

Formation and Rupture of Schottky Nanocontacts on ZnO Nanocolumns

Beatriz Pérez-García,[†] Jesús Zúñiga-Pérez,[‡,§] Vicente Muñoz-Sanjosé,[‡] Jaime Colchero,[†] and Elisa Palacios-Lidón*,[†]

Dep. Física, Edificio CIOyN (Campus Espinardo), Universidad de Murcia, E-30100 Murcia, Spain, and Dpto. Física Aplicada y Electromagnetismo, Universidad de Valencia, C/Dr. Moliner 50, 46100 Burjassot, Spain

Received January 30, 2007; Revised Manuscript Received April 27, 2007

ABSTRACT

In this paper, the electrical transport and mechanical properties of Pt/ZnO Schottky nanocontacts have been studied simultaneously during the formation and rupture of the nanocontacts. By combining multidimensional conducting scanning force spectroscopy with appropriated data processing, the physical relevant parameters (the ideality factor, the Schottky barrier height, and the rupture voltage) are obtained. It has been found that the transport curves strongly depend on the loading force. For loading forces higher than a threshold value, the transport characteristics are similar to those of large-area Schottky contact, while below this threshold deviations from strictly thermionic emission are detected. Above the threshold, stable and reproducible Pt/ZnO nanocontacts with ideality factors of about 2 and Schottky barrier heights of around 0.45 eV have been obtained.

Introduction. With the aim of downscaling semiconductor devices, a big effort has been devoted to growing and controlling semiconductor nanostructures such as nanoparticles, nanowires, or nanobelts. Using these building blocks, nanolasers,[1] nanosensors,[2] nanogenerators,[3] etc. have been already demonstrated. Furthermore, some of the materials employed being biocompatible,[4] nanotechnology has already entered the medicine domain.[2] Most of these applications require, at some point, an electrical contact either to transmit a detected signal or to be powered by an external source. Obviously, the electrical contacts should be scaled accordingly, and therefore, their size must be on the order of nanometers or hundreds of nanometers.

In this context, studying and understanding transport processes at the nanometer scale is essential for an overall improvement of the device response. Especially important for the new applications are Schottky nanocontacts because not only a great number of nanodevices are based on a metal/semiconductor Schottky contact with nanometer dimensions,[3] but also because standard electrical spectroscopies, such as deep level transient spectroscopy or photocurrent measurements, need the formation of a Schottky contact.[5] It is well-known that the behavior of a "small" Schottky nanocontact is different from that of a large-area one.[6−8] Theoretical self-consistent calculations of the electronic structure at the interface predict that if the size of the metal−semiconductor interface is smaller than a characteristic length, proportional to the Debye screening length, the behavior of the contact is governed by its size and shape.[6] Experimentally, it has been found that nanocontacts performed on nanocolumns[9] and nanoislands[10,11] show a strong dependence of the barrier height and ideality factor on their structure as well as on their size.

Some of the main drawbacks related to the studies of electrical transport across Schottky nanocontacts are the lack of control on the contacts formation and their reliability, because it is difficult to measure the mechanical and electrical properties of the nanocontacts simultaneously. In principle, scanning probe microscopies are the ideal tools to overcome these difficulties. With these techniques, it is possible to select the desired regions and then to perform the current voltage *IV* measurements using the conductive tip as a nanoprobe. Several studies have been performed in semiconducting nanostructures by means of conductive scanning force microscopy (c-SFM).[9,12−19] Up to now, the main weaknesses of this technique are the poor characterization of the tip−sample system and, thus, the lack of information on tip and/or sample degradation, as well as the poor mechanical contact stability, due to drift and inherent technical limitations. Under these circumstances, it is difficult to obtain reliable quantitative results because the obtained *IV* curves used to present low reproducibility.[20]

* Corresponding author. E-mail: elisapl@um.es. Telephone: +34 968 39 8554/8273. Fax: +34 968 36 4148.
[†] Dep. Física, Edificio CIOyN (Campus Espinardo), Universidad de Murcia.
[‡] Dpto. Física Aplicada y Electromagnetismo, Universidad de Valencia.
[§] Permanent address: Centre de Recherche sur l'Hétéro-Epitaxie et ses Applications (CRHEA), Centre National de la Recherche Scientifique CNRS, Rue Bernard Grégory, Sophia Antipolis, 06560 Valbonne, France.

10.1021/nl070238m CCC: $37.00
Published on Web 05/19/2007

ZnO is currently one of the most prominent semiconductors for optoelectronic applications due to its large band gap and large exciton binding energy[21] and has become one the most important candidates for spintronics.[22] In this paper, we study in detail the formation and rupture of Schottky nanocontacts on ZnO nanocolumns by means of conductive scanning force spectroscopy (c-SFS). This method combines multidimensional data acquisition, where the *IV* curves and the loading force are recorded simultaneously, with appropriate data processing. In this way, it is possible to analyze in parallel the electrical and the mechanical properties of a nanocontact as a function of the loading force during its formation and rupture. For the nanocontacts studied, formed between a conducting tip and a ZnO nanocolumn, we find that a rectifying behavior is present in all the loading force range. The ideality factor and the barrier height, assuming thermionic emission, as well as the backward rupture voltage, have been calculated. Finally, the results are analyzed in terms of the applied loading force, establishing the existence of a threshold force value above which the contact electrical parameters are constant.

Experimental and Methodology. ZnO was grown at atmospheric pressure in a horizontal metalorganic vapor-phase epitaxy reactor provided with two separate inlets for the zinc and oxygen precursors, diethylzinc and *tert*-butyl alcohol, respectively. This two-inlet configuration allows to avoid, or at least to reduce, gas-phase prereactions between both precursors.[23] ZnO was deposited on $(11\bar{2}0)$ *a*-plane sapphire substrates with the growth direction being parallel to the ZnO *c*-axis. The samples consist of a continuous ZnO film on top of which an array of ZnO nanocolumns develops (see below).

Experiments were performed using a NanoTec SFM system composed of SFM head, high voltage controller, and PLL/dynamic measurement board. In these kinds of experiments, we used sharpened Pt-coated conducting tips with a force constant of 3 or 40 N/m and boron-doped diamond tips with a force constant of 50 N/m. In the experiments discussed here, a platinum tip with a force constant of 3 N/m was used because of its higher force sensitivity as compared to stiffer cantilevers. An ultralow-noise current amplifier (FEMTO LCA-4K-1G) was employed for the conductivity measurements. Experiments have been performed at room temperature under ambient or under a N_2 inert atmosphere. Similar results were obtained under both conditions, nevertheless the data reported in this article are those obtained under N_2 inert atmosphere in order to avoid uncontrolled effects due to formation of water necks.[24] The measurements were performed when the system was sufficiently stable to minimize the drift and to obtain reproducible results. To obtain maximum stability, the microscope setup was kept working for about 24 h before the relevant measurements were performed.

Transport measurements were performed in a three-step sequence: First, topographic images were acquired to select a homogeneous and clean area. Second, the transport properties of the sample were studied by means of c-SFS. Finally, topography images were again acquired to check possible changes in the measured zone.

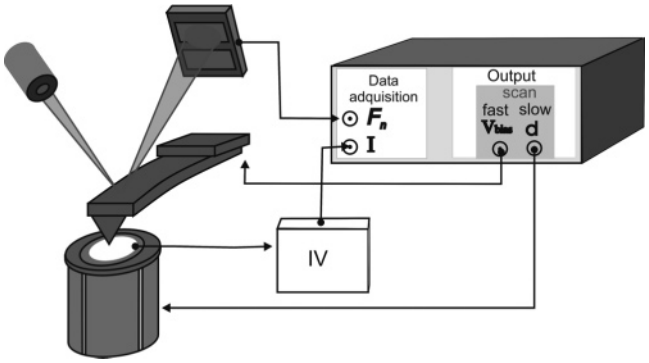

Figure 1. Schematic representation of the experimental setup. In the experiments, the force "*interaction image*" and the "*IV image*" are recorded simultaneously.

As stated before, tip integrity is fundamental in order to obtain reproducible results. In particular, it is important that the tip keeps constant its conducting properties during the whole set of relevant measurements. Mechanical contact of tip and sample may deteriorate the conducting properties of the tip. Therefore, topography images were acquired in true noncontact dynamic scanning force microscopy (DSFM) mode and tip sample contact is established only when performing the transport measurements. Detailed description of DSFM image acquisition is out of the scope of the present paper. We remark, however, that in our experiments, true noncontact imaging is obtained using the oscillation amplitude as a feedback parameter with relatively small oscillation amplitudes (10 nm peak−peak) and a small reduction of oscillation amplitude as a feedback parameter, corresponding to about 90% of the free oscillation amplitude. The phase-locked loop of our dynamic measurement board is enabled to keep the tip−sample system always at resonance. In this way, we work in the attractive regime of tip−sample interaction without touching the surface.

Once the morphology of the samples was obtained, a homogeneous and clean zone was selected for the transport measurements. c-SFS was performed at a given position on the sample as a function of tip−sample voltage V_{bias} and tip−sample distance d: data = data (V_{bias},d). In our SFM system, this acquisition mode is a particular implementation of the 3D mode.[25] The 3D mode was set in order to have the tip voltage as fast scan and the tip−sample distance as slow scan. The experimental implementation of the setup is shown in Figure 1. The outputs (V_{bias},d) from the control unit are supplied to the tip and to the scanner, respectively. In the experiments discussed in this work, the normal force $F(V_{bias},d)$, the frequency shift $\upsilon(V_{bias},d)$, and the oscillation amplitude $A(V_{bias},d)$, as well as the current $I(V_{bias},d)$, are measured simultaneously. The combined set of normal force $F(V_{bias},d)$ and current $I(V_{bias},d)$ data as well as their correlation is the focus of the present study.

Once transport measurements were obtained, the force *"interaction images"* and the *"IV images"* were analyzed with a suitably developed algorithm. A detailed description of the algorithm used to process the force, the frequency,

and the amplitude *"interaction images"* is explained in ref 26. Briefly, first, each line of the force *"interaction image"*, that is, the force measured at a fixed tip−sample distance but at different tip−sample voltages, is averaged over all voltage values to obtain a single force value at that particular tip−sample distance: $F(d) = \sum F(d,U_i)/n$, where the U_i are all voltage points in a (horizontal) data line and n is the total number of points in a line. This process, repeated for each line, converts a force *"interaction image"* into an averaged force vs distance curve (FvsD). This averaged FvsD curve is analogous to the FvsD curves that are typically acquired in scanning force microscopy but has less noise due to the averaging process. The algorithm developed to process the interaction images determines the snap to contact point and separates the contact and noncontact regimes on the FvsD curve. In addition, tip radius, surface potential, and other important parameters are obtained from the noncontact regime data.[26]

The current through the tip for each loading force value, that is, for a fixed tip−sample distance, was collected in the *"IV image"*. Each line of the *"IV image"* corresponds to an *IV* curve at a given point in the FvsD curve. The current curves of the *IV* images were analyzed according to the transport properties of the contact. For contacts with Ohmic behavior (such as Pt/HOPG (highly oriented pyrolitic graphite)), a linear fit was applied to each line of the *IV* image. From each linear fit, the resistance of the tip−sample system at each loading force value was obtained. For contacts with Schottky behavior (such as Pt/ZnO), each *IV* curve was separated into a forward and a backward *IV* branch, corresponding to a positive and a negative tip−sample bias. Assuming the thermionic emission theory (see below),[27] a linear fit was applied to the logarithm of the forward current branch for each loading force. From these fits, the ideality factor and the Schottky barrier height (SBH) were obtained. The breakdown voltage is calculated from the backward current branch. Processing the whole *"IV image"* converts this image to curves describing the variation of ideality factor, SBH, and breakdown voltage with the loading force.

To illustrate the methodology an experiment on a HOPG surface is first discussed. Once a homogeneous and clean area was selected, a metal/metal contact was formed by approaching the tip toward the sample using the 3D mode as discussed before. Data were obtained at a variable bias voltage between −1.4/1.4 V. Approaching force *"interaction image"* and *"IV image"* measurements on HOPG are shown in Figure 2a. In the present context, the analysis is focused on the contact regime. This part of the force *"interaction image"* corresponds to the range in the *"IV image"*, where non-negligible current values are measured. The FvsD curve from the corresponding force *"interaction image"* is shown in Figure 2b.

Current starts to flow through the Pt/HOPG nanocontact when the normal force increases after the minimum of the FvsD curve, which in this case coincides with the beginning of its linear regime. The complete conducting range presents symmetric behavior for both reverse and forward bias

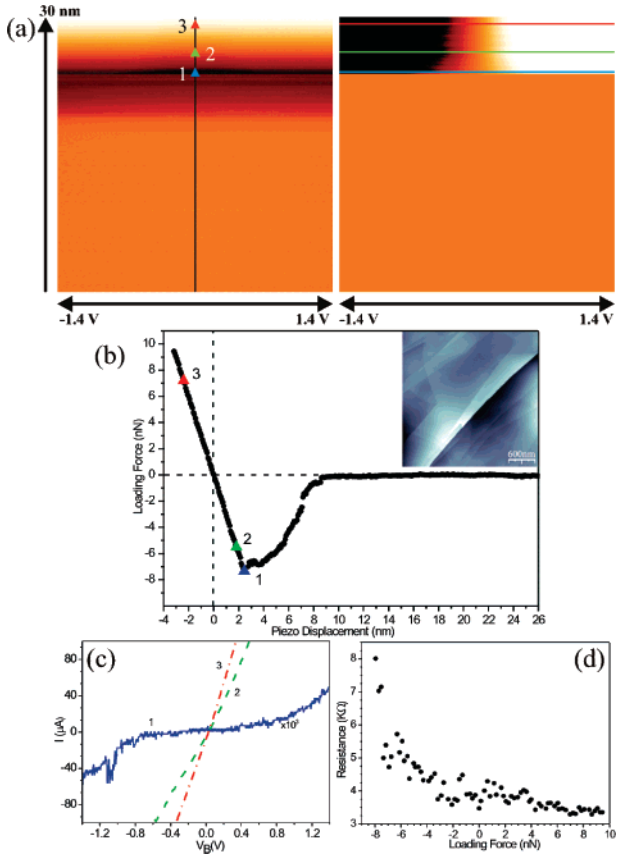

Figure 2. (a) Force "*interaction image*" (left panel) and "*IV image*" (right panel) simultaneously recorded on a HOPG sample. (b) FvsD curve obtained from the force "*interaction image*". A typical DSFM topography image of the HOPG sample is shown in the inset. (c) *IV* curves (1,2,3) at three different loading force values all within the linear range of the FvsD curve. (Also indicated as 1,2,3 in (a) and (b)). (d) Resistance of the tip/sample nanocontact as a function of the loading force.

voltage. For very low loading forces, during the very first stages of tip−sample contact formation, the *IV* curves are nonlinear. Shortly after the minimum of the FvsD curves, at a force value of about −6 nN, the *IV* curves become linear. The corresponding linear fit of the *IV* curves provides the resistance of the tip−sample contact value at each loading force (Figure 2d). As the tip−sample force increases, the resistance decreases until it stabilizes at about 3 kΩ for forces larger than 7 nN. Consequently, a stable and reproducible nanocontact between the tip and the HOPG sample is only formed at sufficiently high loading force values.

The proposed method was employed for determining the transport properties of Schottky nanocontacts on ZnO nanocolumns. To ensure the reliability of the measurements, an additional control step was introduced. Thus, the experiment consists of three consecutive measurements: first, c-SFS was performed on a HOPG surface, then the experiments on the ZnO sample were done, and finally, the control c-SFS measurement on the HOPG sample was repeated. By comparing the two measurements on the HOPG surface, possible variations of the tip can be detected.

Figure 3 shows the morphology of the ZnO sample studied by noncontact DSFM. The sample consists of a thin

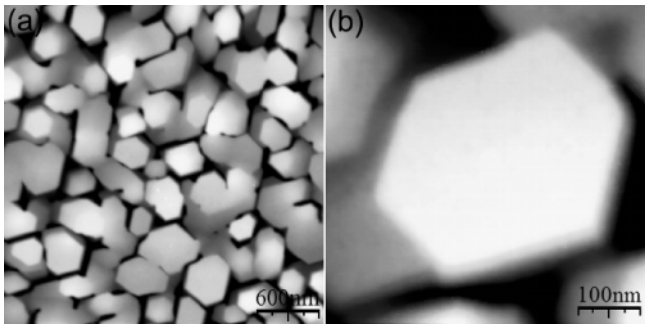

Figure 3. (a) DSFM topography image of the ZnO sample. Array of nanocolumns presenting hexagonal cross sections and flat top endings. (b) Detail of a homogeneous and clean top of a nanocolumn.

continuous ZnO layer that covers the *a*-plane sapphire substrate and an array of ZnO nanocolumns, with lateral sizes between 0.3 and 1 μm, that grow on top of the ZnO layer. Most of the nanocolumns present hexagonal cross sections with flat top endings. This morphology, with flat rather than pyramidal tops, facilitates the formation of stable Pt/ZnO nanocontacts. Hence, only nanocolumns with flat and homogeneous tops were tested.

In analogy to the experiments performed on HOPG, a metal/semiconductor nanocontact was studied by means of c-SFS experiment on a selected ZnO nanocolumn. Silver paste was applied to the bottom of the nanocolumns to electrically connect the ZnO continuous film with the external circuit, similar to ref 3.

A typical c-SFS contact formation experiment on a ZnO nanocolumn is shown in Figure 4, where approaching force "*interaction image*" and "*IV image*" are displayed. Current curves have been acquired at variable bias voltage between −4.5/+4.5 V, thereby measuring forward and reverse *IV* characteristics. Current curves extracted from the "*IV image*" show Schottky rectifying behavior in the whole force range. During the first stages of the nanocontact formation, low forward current and null backward current values are measured.[28] As the loading force increases, both forward and backward currents rise; this trend is maintained until, at a given loading force, the contact properties become constant. The corresponding "*IV image*" acquired during nanocontact rupture (receding tip, not shown) presents the same behavior.

Once the "*IV image*" has been acquired, the forward branch of each *IV* curve is analyzed in terms of thermionic emission theory,[27] according to which the current for positive bias voltage should be given by

$$I(V_{\text{bias}}) = I_s\left[\exp\left(\frac{qV_{\text{bias}}}{nk_BT}\right) - 1\right] \quad (1)$$

where q is the electronic charge, k_B is the Boltzman constant, T the absolute temperature, V_{bias} the applied bias, n the ideality factor, and I_s the saturation current. The algorithm developed for the analysis of the *IV* curves determines the noise level of the current data and then finds the range of

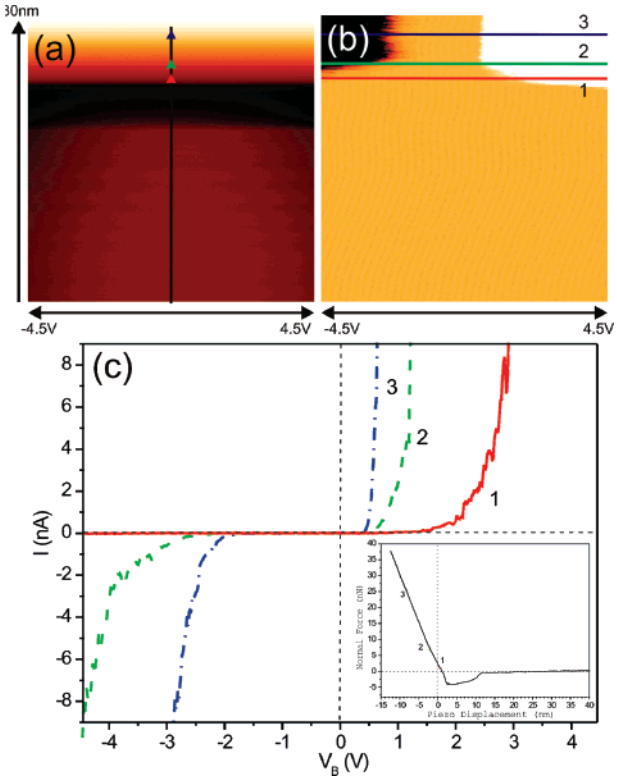

Figure 4. (a) Force "*interaction image*" and (b) "*IV image*" obtained on a ZnO nanocolumn during the nanocontact formation. (c) *IV* curves at three different loading force values (1,2,3). The curves (1,2,3) are also marked in (b). All of them present a clear rectifying behavior.

tip−sample voltages where the current is larger than this noise level and lower than the saturation current of our *IV* converter. When $V_{\text{bias}} \gg k_BT/q$, eq 1 can be simplified to[29]

$$I = I_s\left[\exp\left(\frac{qV_{\text{bias}}}{nk_BT}\right)\right] \quad (2)$$

For each loading force, the ideality factor is then directly determined from the slope of a linear fit $aV_{\text{bias}} + b$ to the experimental data points (V_{bias}, ln(I)). The error of the ideality factor is calculated from the error Δa of the slope of this fit. We note that this "intrinsic" error may be due either to a statistical fluctuation of the data points ("noise") or to a deviation of these data points from the curve that is assumed to be the correct theoretical description of data ("deviation"). The *y*-intercept b of the fit directly gives the logarithm of the saturation current, which is given by

$$I_s = A^*AT^2\exp\left(\frac{q\Phi_B}{k_BT}\right) \quad (3)$$

where A is the area of the diode, Φ_B the SBH of the junction, and A^* the Richardson constant, which for ZnO is 32 A cm^{-2} K^{-2}. The SBH is calculated, according to relations 2 and 3, as:

$$\Phi_B = \frac{k_B T}{q}\{b - \ln(A^*) - \ln(A) - 2\ln(T)\} \quad (4)$$

The corresponding error is

$$\Delta\Phi_{Bs} = \frac{k_B T}{q}\sqrt{\left(\frac{\Delta b}{b}\right)^2 + \left(\frac{\Delta A}{A}\right)^2 + 2\left(\frac{\Delta T}{T}\right)^2} \quad (5)$$

which in our case can be simplified to $\Delta\Phi_B = (k_B T/q)(\Delta b/b)$ because the error of the saturation current is the leading error source in our experiments.

Finally, the reverse breakdown voltage as a function of the loading force is obtained from the backward *IV* branch. As for the forward *IV* curve, the noise level of the current data is determined. In our case, we define the breakdown voltage as the voltage for which the reverse current is larger than twice the noise level.

Results. The ideality factor of the Pt/ZnO nanocontact during its formation is shown in Figure 5a. The ideality factor decreases from about 15 at very low loading forces to about 2 at loading forces higher than about 10 nN and remains essentially constant for higher forces. Taking into account the (intrinsic) error of each point on the ideality vs distance curve and the dispersion of these points,[30] the nanocontact formation can be separated into three regions: in the first one (I), for loading forces lower than 5 nN, the points on the ideality factor vs distance curve present high dispersion and a relatively large "intrinsic" error which is of essentially statistical nature (noise). This range corresponds, most probably, to an unstable electric nanocontact that is still under formation.[20] In the second region (II), for loading forces between 5 and 10 nN, the ideality factors present lower dispersion and their "intrinsic" error is due to "deviation", that is, the *IV* curves in this regime are not well described by simple exponential functions. Finally, at loading forces higher than 10 nN (region III), the ideality factor vs distance curve shows very low dispersion, is essentially constant and has low error bars. In particular, in this regime, the *IV* curves are described by eq 1. In this regime, a stable electric contact has been already formed. This trend is completely reproducible both in the formation and in the rupture of the nanocontact (parts a and b of Figure 5, respectively), although the first and second regions are less well defined and noisier during the rupture process.

The obtained ideality factor is much lower than those previously reported, ranging between 6 and 12, on ZnO[9,16−18] and GaN[19] nanocolumns contacted with an AFM tip. These high ideality factors were attributed to small contact size effects and agree with our results obtained at low loading forces. On the other hand, it is noteworthy that, in the third loading force region, where a stable nanocontact has been formed, the ideality factors that we systematically obtain are much lower (∼2). This ideality factor matches the best value recently obtained on large-area Pt Schottky contacts on Zn-polar bulk ZnO,[31] confirming that high-quality nanocontacts can be obtained by the present method. Furthermore, the diode characteristics and, in particular, the ideality factor were seen to depend on the particular polarity of the ZnO surface contacted[31] as well as on the surface treatment employed before depositing the Pt contact.[15] Thus, an improvement of the nanocontact characteristics should be achievable by employing O-polar surfaces or by exposing the ZnO surface to boiling hydrogen peroxide.

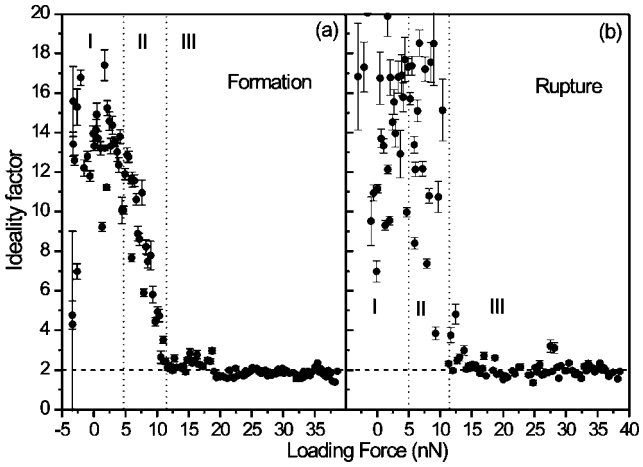

Figure 5. Ideality factor as a function of the loading force for (a) formation and (b) rupture of the Pt/ZnO nanocontact. The three regions explained on the main text are indicated as I, II, and III in the graphs.

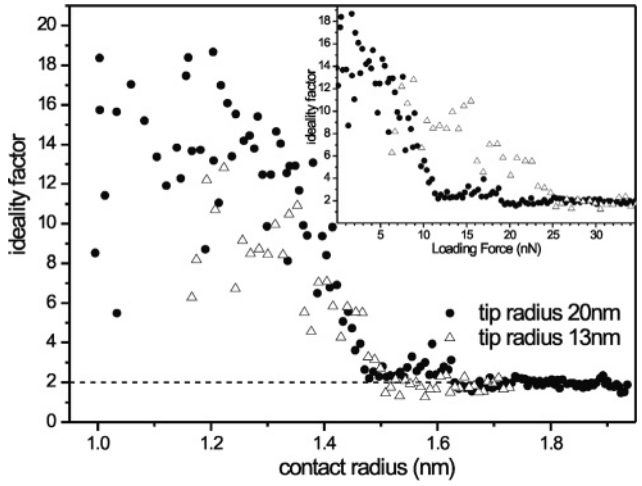

Figure 6. Ideality factor as a function of the contact radius for two Pt tips. Inset: Ideality factor as a function of the loading force of the same two Pt tips.

To check the reproducibility of the experiment and the dependence of the ideality factor with the contact radius, measurements have been repeated using different platinum tips. The ideality factor as a function of the loading force for two different tips is displayed in the inset of Figure 6. It is clearly seen that, although both tips show the same trend, the threshold loading force, above which the ideality factor reaches a constant value, is quite different for each tip. Instead of using the loading force, it is very enlightening to study the dependence of the ideality factor on the contact radius (Figure 6). For this purpose, the contact radii have been calculated using the Derjaguin−Muller−Toporov (DMT) model,[32] which describes the contact radius between a spherical tip (of tip radius R) and a flat surface when both bodies are pushed into each other. As compared to the

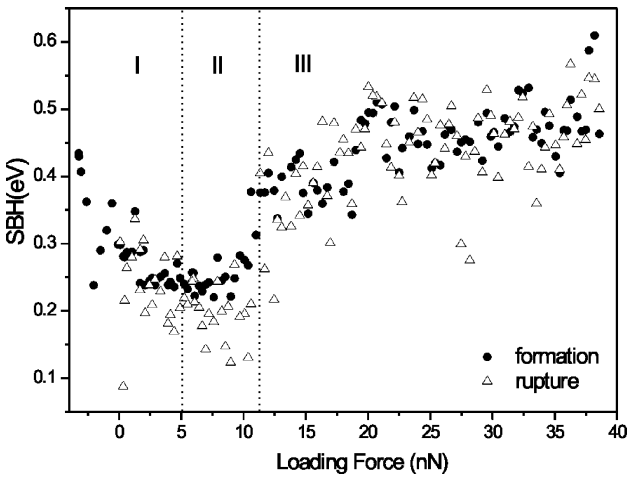

Figure 7. Schottky barrier height Φ_B as a function of the loading force is shown. The error bars (not shown) are about 0.2 eV. This large value is because the low saturation currents are smaller than the technical noise of our measurements.

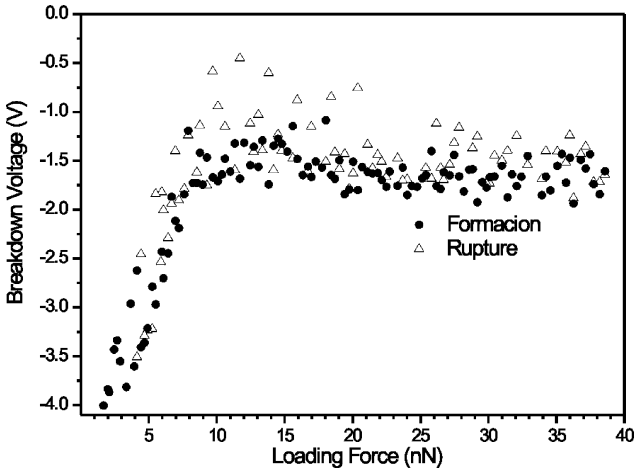

Figure 8. Breakdown voltage as a function of the loading force.

simpler Hertz model, this model takes into account the adhesion forces acting in the tip−sample contact as well as the elasticity of tip and sample. For a spherical tip on a flat surface, the contact area will be a circle whose radius increases with the loading force.

The contact radius is then given by $a = \sqrt[3]{(R/E)(F+|F_{adh}|)}$, where R is the tip radius obtained from the analysis of the frequency *"interaction image"* in the noncontact regime, as extensively explained in ref 26, E the effective Young's modulus of the tip (about 134 GPa), F the loading force, and F_{adh} the adhesion force, which in our experiments is about 10 nN, as estimated from the FvsD curves. Contact radii of a few nanometers (1−3 nm) have been obtained for all the tips within the force range investigated experimentally in this work. As shown in Figure 6, the ideality factor obtained with different tips, but the same tip material, as a function of the contact radius, shows strong coincidence. On the other hand, similar experiments performed with highly doped diamond tips (not shown here) present the same behavior but with a saturation value of the ideality factor of about 2.8. This clearly indicates that the ideality factor depends on the tip material.

Another important parameter to characterize a Schottky contact is the SBH, which is obtained from eq 4. The SBH as a function of the loading force is shown in Figure 7. At low loading forces, where the nanocontact is still under formation, although the SBH values show large dispersion, they seem to decrease. For loading forces higher than 5 nN, the SBH increases as the loading force rises, increasing from about 0.2 eV to about 0.45 eV at loading forces higher than 20 nN when a stable nanocontact has been formed. This behavior is followed both in the formation and in the rupture of the nanocontact with good agreement, although the rupture curve is again noisier. The experimental SBH values (∼0.45 eV) obtained at loading forces higher than a threshold value are close to those found in Pt/ZnO large-area Schottky contacts (∼0.55 eV).[31] At low loading forces, the measured SBH values are obviously smaller.

Finally, to fully characterize the *IV* curves, the breakdown voltage has been obtained by processing the reverse *IV* curves with a suitable algorithm. The corresponding breakdown voltage as a function of the loading force is shown in Figure 8. Non-negligible backward currents are only obtained for forces higher than 1 nN. For loading forces between 1 and 10 nN, the breakdown voltage decreases as the loading force increases, from more than −4.5 V up to a value of about −1.75 V. For loading forces higher than 10 nN, the breakdown voltage stays constant at this value. This breakdown voltage is much lower than those typically found in large-area Schottky contacts and is probably a result of the small size of the nanocontact, as will be discussed below.

Discussion and Conclusions. It is important to notice that, for all experiments described here, the contact radius variation during the transport experiments is very small, typically 1−4 nm. This is fundamental in the present discussion because "small" nanocontacts are expected to deviate from conventional diodes behavior. As discussed in ref 6, a nanocontact should be considered "small" if its radius is smaller than or similar to the characteristic length of the system, which is proportional to the Debye screening length. In nonintentionally doped ZnO samples, such as those used in this study and comparable to those studied previously,[9] the doping level is about $10^{17}-10^{18}$ cm^{-3} and, therefore, the corresponding Debye lengths are on the order of 3−10 nm. This would mean that our nanocontacts are "small" and the corresponding size effects should play an important role. The large ideality factors and low SHB found in the region II could therefore be explained by taking into account these effects as previously done in other similar structures.[9,15,16] However, it should be emphasized that, in our experiments, the transition between the second and the third regime, where the ideality factor and the barrier height are constant, is extremely sharp (compare with Figure 1 in ref 6). In addition, in regime III, the transport characteristics can be fully described by thermionic emission (and the series resistance of the structure). Therefore, nanocontacts with ideality factors and SHB comparable to large-area Schottky contacts can be formed even though, in principle, "small" size effects should be relevant. Besides, transport measurements performed with

c-SFM on $TiSi_2$ islands on Si(111), previously reported in ref 12, showed that the current characteristics were not correlated with the island size but with the quality of the metal/semiconductor interface. In our case, similar effects could take place and, thus, a high-quality Pt/ZnO interface would not be achieved until a certain threshold force is applied.

The rupture voltages are in all the cases much lower than the large-area contact ones. This effect would be similar to that produced by a reduced barrier width, as introduced in ref 6, to simulate small contact size effects because it would increase the tunneling of carriers across the barrier and produce an enhancement of the backward current. Furthermore, even if the use of an inert nitrogen atmosphere should prevent, or at least reduce, the formation of surface conducting channels, their presence should not be completely discarded.

We would like to highlight that one of the main efforts in our work has been to accurately determine the errors in all our experiments. In particular, it has been very important to assign an "intrinsic" error to the calculated *IV* curves, enabling us to recognize deviations from the ideal Schottky diode behavior (region II of ideality vs distance curves) and to discriminate among the results having very low dispersion (region III of ideality vs distance curves). Finally, we have shown that, because relatively small variations on the mechanical properties of the nanocontact can induce a dramatic change of its transport properties, a high control on the formation and rupture of the nanocontact is crucial to understand electrical transport across it.

In summary, the ideality factor, the SBH, and the rupture voltage of Schottky nanocontacts created on ZnO with Pt SFM tips have been studied during the formation and rupture of the nanocontact. We have combined multidimensional c-SFS data acquisition with appropriate processing algorithms to characterize the mechanical and electrical behavior of these nanocontacts. A detailed analysis of the experimental data acquired during the evolution of the process shows that, at low loading forces, the *IV* characteristics cannot be explained with simple thermionic theory. This anomalous behavior could be due either to the small size of the nanocontact, similarly to previous measurements on ZnO nanostructures, as well as a poor tip−sample interface. Above a threshold loading pressure, a stable nanocontact is formed and the ideality factor, as well as the SBH, attain similar values to those obtained on large-area Pt/ZnO Schottky contacts. We believe that the methodology developed in the present study will be a step forward in the field and paves the way for further and deeper understanding of electrical transport trough nanocontacts.

Acknowledgment. We thank Dr. J. Abellán for technical assistance and H. von Wenckstern for stimulating discussions. This work has been supported by the Spanish government under projects MAT2004-06841, MAT2005-23915E, NAN2004-09183-C10-3, GV-Grupos 03/098, GV-Comp 2006-0037, and the Fundación Séneca-CARM.

References

(1) Huang, M.; Mao, S.; Feick, H.; Yan, H.; Wu, Y.; Kind, H.; Weber, E.; Russo, R.; Yang, P. *Science* **2001**, *292*, 1897.
(2) Patolsky, F.; Lieber, C. M. *Mater. Today* **2005**, *8*, 20.
(3) Wang, Z. L.; Song, J. *Science* **2006**, *312*, 243.
(4) Zhou, J.; Xu, N.; Wang, Z. L. *Adv. Mater.* **2006**, *18*, 2432.
(5) von Wenckstern, H.; Pickenhain, R.; Schmidt, H.; Brandt, M.; Biehne, G.; Lorenz, M.; Grundmann, M. *Appl. Phys. Lett.* **2006**, *89*, 092122.
(6) Smit, G. D. J.; Rogge, S.; Klapwijk, T. M. *Appl. Phys. Lett.* **2002**, *81*, 3852.
(7) Hägglund, C.; Zhdanov, V. P. *Physica E* **2006**, *33*, 296.
(8) Osvald, J. *Solid State Comun.* **2006**, *138*, 39.
(9) Park, W. I.; Yi, G. C.; Kim, J. W.; Park, S. M. *Appl. Phys. Lett.* **2003**, *82*, 4358.
(10) Smit, G. D. J.; Rogge, S.; Klapwijk, T. M. *Appl. Phys. Lett.* **2002**, *80*, 2568.
(11) Hugekman, M.; Schindler, W. *Appl. Phys. Lett.* **2004**, *85*, 3608.
(12) Oh, J.; Nemanich, R. J. *J. Appl. Phys.* **2002**, *92*, 3326.
(13) Spradlin, J.; Dogan, S.; Xie, J.; Molnar, R.; Baski, A. A.; Morkoc, H. *Appl. Phys. Lett.* **2004**, *84*, 4150.
(14) Heo, Y. H.; Tien, L. C.; Norton, D. P.; Pearton, S. J. *Appl. Phys. Lett.* **2004**, *85*, 3107.
(15) Kim, S. H.; Kim, H. K.; Seong, T. Y. *Appl. Phys. Lett.* **2005**, *86*, 112101.
(16) Pan, N.; Wang, X.; Zhang, K.; Hu, H.; Xu, B. *Nanotechnology* **2005**, *16*, 1069.
(17) Fan, Z.; Dutta, D.; Chien, C. J.; Chen, H. Y.; Brown, E. C.; Chang, P. C.; Lu, J. G. *Appl. Phys. Lett.* **2006**, *89*, 213110.
(18) Pradhan, B.; Batabyal, S. K.; Pal, A. J. *Appl. Phys. Lett.* **2006**, *89*, 233109.
(19) Deb, P.; Kim, H.; Qin, Y.; Lahiji, R.; Oliver, M.; Reifenberger, R.; Sands, T. *Nano Lett.* **2006**, *6*, 2893.
(20) Guo, D. Z.; Hou, S. M.; Zhang, G. M. Xue, Z. Q. *Appl. Surf. Sci.* **2006**, *252*, 5149.
(21) Özgur, Ü.; Alivov, Y. I.; Liu, C.; Teke, A.; Reshchikov, M. A.; Dogan, S.; Avrutin, V.; Cho, S. J.; Morkoç, H. *J. Appl. Phys.* **2005**, *98*, 041301.
(22) Dietl, T.; Ohno, H.; Matsukura, F.; Cibert, J.; Ferrand, D. *Science* **2000**, *287*, 1019.
(23) Tena-Zaera, R.; Zúñiga-Pérez, J.; Martinez-Tomas, C.; Muñoz-Sanjosé, V. *J. Cryst. Growth* **2004**, *264*, 237.
(24) Luna, M.; Colchero, J.; Gil, A.; Gómez-Herrero, J.; Baró, A. M. *Appl. Surf. Sci.* **1999**, *157*, 285−289.
(25) Gómez-Navarro, C.; Gil, A.; Álvarez, M.; De Pablo, P. J.; Moreno-Herrero, F.; Horcas, I.; Fernández, R.; Colchero, J.; Gómez-Herrero, J.; Baró, A. M. *Nanotechnology* **2002**, *13*, 314.
(26) Palacios-Lidón, E.; Colchero, J. *Nanotechnology* **2006**, 17, 5491.
(27) Sze, S. M. *Physics of Semiconductor Devices*; Wiley: New York, 1981.
(28) The detection limit of our system is about 20 pA.
(29) The correct relation justifying the approximation leading to eq 2 is $V_{bias} \gg 3nk_BT/q$, where n is the ideality factor. For large n, as those found in previous Schottky nanocontacts, the validity of this inequality should be carefully analyzed.
(30) With "intrinsic" error, we mean the error bars calculated from the processing of a line of data points from the *IV* image, while dispersion means how the points of the ideality factor vs distance curve vary with respect to the local trend of the points. Thus, dispersion is essentially the fluctuation of the ideality factor vs distance curve.
(31) Allen, M. W.; Alkais, M. M.; Durbin, S. M. *Appl. Phys. Lett.* **2006**, *89*, 103520.
(32) Derjaguin, B. V.; Müller, V. M.; Toporov, Y. P. *J. Colloid Interface Sci.* **1975**, *53*, 314; Müller, V. M.;. Yushchenko, V. S.; Derjaguin, B. V. *J. Colloid Interface Sci.* **1980**, *77*, 91; Müller, V. M.; Derjaguin, B. V.; Toporov, Y. P. *Colloids Surf.* **1983**, *7*, 251.

NL070238M